BIOCHEMISTRY
including biophysical chemistry & molecular biology

Article

pubs.acs.org/biochemistry

Control of Cyclic Photoinitiated Electron Transfer between Cytochrome *c* Peroxidase (W191F) and Cytochrome *c* by Formation of Dynamic Binary and Ternary Complexes

Taylor R. Page and Brian M. Hoffman*

Department of Chemistry, Northwestern University, 2145 Sheridan Road, Evanston, Illinois 60208-3113, United States

Supporting Information

ABSTRACT: Extensive studies of the physiological protein−protein electron-transfer (ET) complex between yeast cytochrome *c* peroxidase (CcP) and cytochrome *c* (Cc) have left unresolved questions about how formation and dissociation of binary and ternary complexes influence ET. We probe this issue through a study of the photocycle of ET between Zn-protoporphyrin IX-substituted CcP(W191F) (ZnPCcP) and Cc. Photoexcitation of ZnPCcP in complex with Fe^{3+}Cc initiates the photocycle: charge-separation ET, [^{3}ZnPCcP, Fe^{3+}Cc] → [ZnP^+CcP, Fe^{2+}Cc], followed by charge recombination, [ZnP^+CcP, Fe^{2+}Cc] → [ZnPCcP, Fe^{3+}Cc]. The W191F mutation eliminates fast hole hopping through W191, enhancing accumulation of the charge-separated intermediate and extending the time scale for binding and dissociation of the charge-separated complex. Both triplet quenching and the charge-separated intermediate were monitored during titrations of ZnPCcP with Fe^{3+}Cc, Fe^{2+}Cc, and redox-inert CuCc. The results require a photocycle that includes dissociation and/or recombination of the charge-separated binary complex and a charge-separated ternary complex, [ZnP^+CcP, Fe^{2+}Cc, Fe^{3+}Cc]. The expanded kinetic scheme formalizes earlier proposals of "substrate-assisted product dissociation" within the photocycle. The measurements yield the thermodynamic affinity constants for binding the first and second Cc: $K_I = 10^{-7}$ M^{-1}, and $K_{II} = 10^{-4}$ M^{-1}. However, two-site analysis of the thermodynamics of formation of the ternary complex reveals that Cc binds at the weaker-binding site with much greater affinity than previously recognized and places upper bounds on the contributions of repulsion between the two Cc's of the ternary complex. In conjunction with recent nuclear magnetic resonance studies, the analysis further suggests a dynamic view of the ternary complex, wherein neither Cc necessarily faithfully adopts the crystal-structure configuration because of Cc−Cc repulsion.

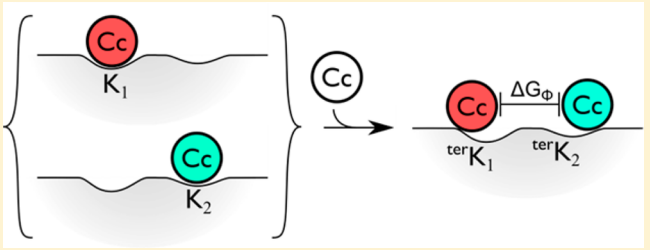

The complex between the physiological protein−protein electron-transfer (ET) partners yeast cytochrome *c* peroxidase (CcP) and cytochrome *c* (Cc) was the first ET-active complex to be crystallized and remains a paradigm for ET within a well-defined complex.[1] Despite extensive studies of this pair by nuclear magnetic resonance (NMR),[2−4] crystallography,[5,6] photoinduced kinetic measurements,[7−9] and other spectroscopic techniques,[10−12] there nonetheless remain fundamental questions about how ET between them is modulated by the formation and dissociation of the complex on the ET time scale and about the possible role of a ternary complex in reactivity.[4] The pair has been particularly amenable to study because the heme iron of either partner can be substituted with Zn (or Mg) to form a complex that exhibits an ET photocycle.[8] When the Fe of CcP is substituted to form ZnPCcP and is in a complex with the iron form of the partner protein, Fe^{3+}Cc, the complex can undergo a laser-initiated ET photocycle comprised of "forward" charge-separation (CS) ET (^{3}ZnPCcP;Fe^{3+}Cc → ZnP^+CcP;Fe^{2+}Cc), with rate constant k_f, to produce the charge-separated intermediate protein pair, ZnP^+CcP and Fe^{2+}Cc (denoted **I**, representing all states involving ZnP^+CcP) followed by "back" charge-recombination (CR) ET to regenerate the initial state (ZnPCcP;Fe^{3+}Cc ← ZnP^+CcP;Fe^{2+}Cc) with rate constant k_b,[13] a process analogous to physiological ET wherein Fe^{2+}Cc reduces CcP Compound ES.

The CR process in the complex formed with ZnP-substituted, wild-type CcP is extremely rapid ($k_b \sim 3500$ $s^{-1} \gg k_f$) because CcP residue tryptophan 191 on the proximal side of the heme "short-circuits" direct heme−heme "back" ET via "hole hopping" in which the ZnP^+ oxidizes W191 and the $W191^{+\bullet}$ cation radical oxidizes Fe^{2+}Cc. This process makes it difficult to examine the behavior of the CS intermediate, **I**, and altogether precludes examination of the dynamic processes within **I** on longer time scales.[8,14−17] To fully explore the role of complex formation/dissociation dynamics in the ET photocycle, we employ CcP W191F; this mutation negligibly perturbs the overall structure of CcP[18] and does not impact the ability of Fe^{3+}Cc to quench ^{3}ZnPCcP but prevents the short-circuit and slows CR.[9] The [ZnPCcP(W191F), Fe^{3+}Cc]

Received: July 18, 2014
Revised: January 14, 2015
Published: January 28, 2015

DOI: 10.1021/bi500888y
Biochemistry 2015, 54, 1188−1197

complex thus is well-suited for studying direct interprotein heme−heme ET, and its use allows us to monitor **I** over a wide range of time scales.[9]

In this study, the charge-separated intermediate was monitored through titrations of ZnPCcP by Fe^{3+}Cc, Fe^{2+}Cc, and redox-inert CuCc.[19] These studies allow a detailed examination of the dynamics of formation and dissociation of the binary [CcP, Cc] complex, revealing the importance of the charge-separated ternary complex, **I**3(2+/3+) ≡ [ZnP^{+}CcP, Fe^{2+}Cc, Fe^{3+}Cc].[a] These findings are incorporated into an extended kinetic mechanism for the ET photocycle between ZnPCcP(W191F) and yeast Iso-1 Fe^{3+}Cc that formalizes and enhances earlier proposals of "substrate-assisted product dissociation",[20] by incorporation of a dynamic ternary complex.[21]

The measurements of CS further yield the consensus values of the thermodynamic affinity constants for binding the first and second Cc. However, a two-site analysis of the thermodynamics of formation of the ternary complex that explicitly incorporates repulsion between the two Cc's reveals that Cc binds at the weaker-binding site with much greater affinity than previously recognized and places upper bounds on the free energy of repulsion between the two Cc's of the ternary complex. In conjunction with recent descriptions of the equilibrium between encounter and docked complexes,[22,23] the analysis further suggests a modified view of the ternary complex's structure, as a dynamic association of CcP and two Cc's wherein neither Cc necessarily adopts the crystal-structure configuration because of Cc−Cc repulsion.

MATERIALS AND METHODS

Protein Preparation. The recombinant yeast cytochrome *c* peroxidase (CcP) W191F mutant based on the MKT construct and recombinant yeast Iso-1 cytochrome *c* (Cc) were isolated and purified using previously published protocols.[24,25] The holoenzyme CcP purity was assayed using a 408 nm/282 nm ratio of 1.3 and sodium dodecyl sulfate−polyacrylamide gel electrophoresis (SDS−PAGE). ApoCcP was prepared and subsequently reconstituted with Zn-protoporphyrin IX in the dark as previously described,[26] and the purity was assayed using a 432 nm/282 nm ratio of >3 and SDS−PAGE. To prepare metal-free Cc, in a chemical hood, 3−10 mL of pyridine-HF was added to ∼100 mg of lyophilized FeCc in a polyethylene beaker and gently stirred in the dark with a magnetic stirrer for 10 min with a stream of nitrogen blowing over the surface. The reaction was quenched with 10 mL of 50 mM acetate buffer (pH 5) and the mixture allowed to stir gently for 30 min with nitrogen blowing over the surface. Appropriate HF respirators, gloves, laboratory coats, and aprons were used at all times when HF was in use. Excess Fe and pyridine were removed using a short Sephadex G-50 column. Metal-free Cc was diluted by half with water and loaded onto a short Whatman CM52 column equilibrated with 25 mM acetate buffer (pH 5). The column was washed extensively with buffer to remove pyridine and eluted with 25 mM acetate, 500 mM NaCl buffer (pH 5). CuCc was prepared from metal-free Cc as previously described.[27]

Kinetic Measurements. Transient absorption kinetic measurements were performed on a laser flash-photolysis apparatus described elsewhere. Wild-type and mutant FeCc were freshly oxidized with an at least 10-fold excess of potassium ferricyanide the day of the experiments. Excess potassium ferricyanide was removed by passing the Fe^{3+}Cc and potassium ferricyanide solution through a 2 mL CM-52 column preequilibrated with water. Fe^{3+}Cc was eluted using 500 mM NaCl, 25 mM KP_i buffer (pH 7). Proteins were exchanged into potassium phosphate buffers and concentrated using ultracentrifugation. Protein stocks were flushed with argon using a Schlenk line prior to addition and transferred to sample cuvettes using Hamilton gastight syringes 30 min before the experiments to allow for further oxygen scrubbing. For all samples, the day before the experiments, 2.00 mL of buffer in an airtight quartz cuvette was flushed with argon for 1 h using a Schlenk line after which a catalase oxygen-scavenging system was added to ensure complete deoxygenation (final concentrations of 10 μM catalase, 10 μM glucose oxidase, and 10 μM glucose). Concentrations were determined using the following values: ε_{432} = 196 mM^{-1} cm^{-1} for ZnPCcP, ε_{409} = 106 mM^{-1} cm^{-1} and ε_{416} = 129 mM^{-1} cm^{-1} for Fe^{3+}Cc and Fe^{2+}Cc, respectively, and ε_{422} = 138 mM^{-1} cm^{-1} for CuCc.

Model Simulation and Fitting. Global fits of titration kinetic traces to analytical expressions and numerical fits to the set of kinetic differential equations were calculated with MATLAB using routines written in house. Numerical integration of the set of differential equations for Scheme 1 (*vide infra*) employed the MATLAB ode45 solver [which uses the explicit Runge−Kutta (4,5) formula, Dormand−Prince pair]. The 95% confidence intervals for the kinetic parameters were calculated with the built-in *nlparci* function in MATLAB. Details of the differential equations and global fitting equations are presented in the Supporting Information.

RESULTS

Low-Salt (10 mM KP_i) Fe^{3+}Cc Titration. *ET Quenching.* Fe^{3+}Cc was titrated into a sample of ∼5 μM ZnPCcP(W191F) in 10 mM KP_i buffer (pH 7) at 20 °C. In the absence of Fe^{3+}Cc, ^{3}ZnPCcP decays exponentially with a k_1 of ≈90 s^{-1}. With further additions of Fe^{3+}Cc, the triplet state decay traces can be described with a double-exponential function with decay constants (k_1 ≈ 90 s^{-1}, and k_2 ≈ 320 s^{-1}) and fractions f_1 and f_2, respectively, with initial amplitude A_0.[b] As long as 0 < [Fe^{3+}Cc] < $[ZnPCcP]_0$, k_1 and k_2 are nearly unchanged while f_2 increases nearly linearly, as appropriate for a tightly bound 1:1 complex in slow exchange with its dissociated components;[28] at the titration end point, when [Fe^{3+}Cc] ≈ $[ZnPCcP]_0$, and the formation of a binary is roughly complete (f_2 ≈ 1), the triplet decay is approximately exponential with a k_2 of ∼320 s^{-1}. However, past this point, when [Fe^{3+}Cc] > $[ZnPCcP]_0$, the triplet decay again becomes biexponential with the appearance of a faster phase, decay constant k_3, associated with the formation of a 2:1 complex in slow exchange with the 1:1 complex, with enhanced quenching in the ternary complex: ternary quenching rate constant (k_3 > k_2). A correlation between the yield of the charge-separated intermediate (see below) and the rate constant for quenching suggests than much of the quenching in the ternary complex is by energy transfer.

To incorporate both binary and ternary complexes, the triplet decay traces were fit with a triple-exponential function (Figure S1 of the Supporting Information), which corresponds to a model in which equilibrium populations of free, 1:1, and 2:1 complexes are in slow exchange and decay independently. To test this protocol and to further reduce the total number of fit parameters, the entire set of triplet decay traces was also fit globally to rate constants k_1, k_2, and k_3 and affinity constants K_I and K_{II}. Although the two fitting approaches give comparable values, the confidence intervals for the global approach are better (smaller). The values of the rate constants and affinity

DOI: 10.1021/bi500888y
Biochemistry 2015, 54, 1188−1197

constants obtained in this fashion are listed in Table 1 and are consistent with previous reports.[8,9]

Table 1. $Fe^{3+}Cc$ Titration Triplet Decay Kinetic Parameters[a]

k_1	89.7 ± 0.2 s^{-1}
k_2	297 ± 0.7 s^{-1}
k_3	1190 ± 63 s^{-1}
K_I	(2.3 ± 0.2) × 10^7 M^{-1}
K_{II}	(9.2 ± 0.3) × 10^3 M^{-1}

[a]Parameters shown with 95% confidence intervals.

Charge-Separated Intermediate. The progress curves of the charge-separated intermediate state (**I**) were followed through an $Fe^{3+}Cc$ titration by monitoring the transient absorbance upon photolysis at a ^{3}ZnPCcP − ground isosbestic, 445 nm, a wavelength where both the ZnP^+CcP − ZnPCcP and $Fe^{2+}Cc$ − $Fe^{3+}Cc$ absorbance differences contribute to the transient absorbance. As with the quenching measurement, the behavior of **I** is not consistent with a simple 1:1 stoichiometry in slow exchange. If charge separation and recombination occurred as a simple, intracomplex photocycle, one would expect a simple exponential rise and fall for the absorbance of **I**, with *unchanging* rate constants throughout the titration, one corresponding to the intracomplex triplet decay constant and the other to intracomplex CR associated with the return of **I** to ground; only the signal amplitude would change during a titration.

Instead, although we observe an increase in the maximal level of accumulation of **I**,[c] the shapes of the progress curves for **I** are complex, with an apparently exponential rise and biphasic fall, one exponential phase decaying within ∼50 ms and the other, a second-order phase, decaying only over 1 s or longer, with the proportions of the slower phase increasing during the course of the titration (Figure 1). Throughout the titration, plots of the

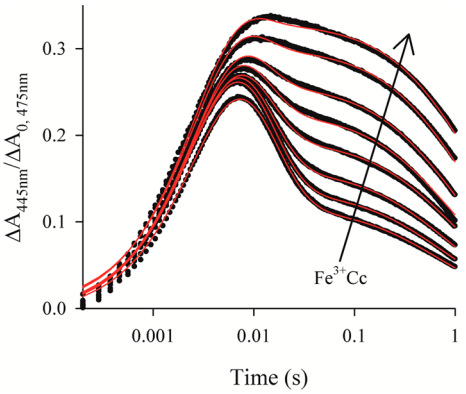

Figure 1. Titration of a sample of ∼5 μM ZnPCcP with $Fe^{3+}Cc$ (5−26 μM). Progress curves for the charge-separated intermediate (black) normalized to A_0 for the corresponding triplet decay curves with fits to Scheme 1 (red). Conditions: 10 mM KP_i buffer (pH 7), 20 °C.

reciprocals of the absorbance difference are linear at times where it is dominated by the slow component (Figure 2), which shows that this phase of CR is second-order. Indeed, any description of the slow phase in the recovery of the ground state must incorporate dissociation and recombination of **I**: the complex could not remain bound for the duration of the intermediate signal, ∼1−2 s. For **I** to remain just 90% bound for at least 1 s, the dissociation rate constant would need to be

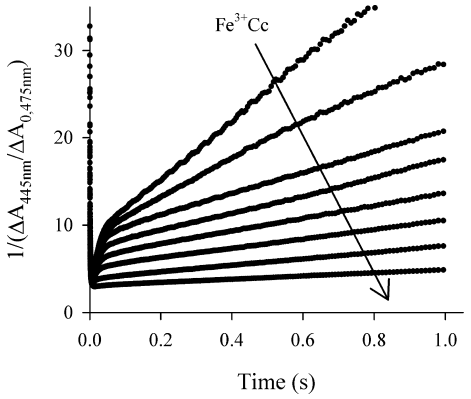

Figure 2. Titration of a sample of ∼5 μM ZnPCcP with $Fe^{3+}Cc$ (5−26 μM). Reciprocal absorbance plots of the progress curves for charge separation measured at 445 nm.

≤0.1 s^{-1}, which is 2 orders of magnitude smaller than that calculated using the measured binding constant (K_I = 2 × 10^7 M^{-1}), and the reported association rate constant (k_{on}) of at least ∼10^8 M^{-1} s^{-1}.[29]

The results to this point indicate that two extensions of the simple photocycle are required. The results of the $Fe^{3+}Cc$ quenching titration clearly indicate the formation of a ternary complex in the triplet state, and thus presumably in **I**, as well; the behavior of the CR shows that the description must furthermore incorporate dissociation and reassociation of the charge-separated intermediate complex, [ZnP^+CcP, $Fe^{2+}Cc$] ≡ **I**2(2+). However, these "simple" extensions profoundly complicate the kinetic scheme for a photocycle. A full kinetic scheme that incorporates binary and ternary complexes of the triplet state and **I**, as well as dissociation and reassociation of each species in all possible combinations, is presented in Scheme S1 of the Supporting Information. This scheme includes 18 species, 36 equilibrium processes, and at least six ET processes. Clearly, it is not practicable to determine all the parameters in such a scheme. However, it is possible to assess the roles of dissociation and of the ternary charge-separated complexes in the CR process and determine key kinetic parameters by considering successively more complex *sub-schemes* extracted from Scheme S1 of the Supporting Information, beginning with a *minimal* kinetic subscheme described previously[9] (Scheme 1) and then including additional kinetic routes as needed to arrive at a *core* model (presented below as Scheme 2) that captures the key features needed to describe the progress curve for **I**.

Minimal Kinetic Scheme. To begin, we recognize that although a full fit to the triplet decay traces requires a 2:1 binding model, the majority of bound ^{3}ZnPCcP exists as the binary complex even at the highest [$Fe^{3+}Cc$]. Therefore, Scheme 1 includes only the dominant channel for intracomplex photoinitiated CS, [^{3}ZnPCcP, $Fe^{3+}Cc$] → [ZnP^+CcP, $Fe^{2+}Cc$]. These measurements cannot yield meaningful parameter values for minor channels, as the small contributions from such channels are overwhelmed by the smallest deviations from the triplet/ground isosbestic, where the measurements must be made, and where the absorbance difference for **I** is not maximal. Once formed, **I**2(2+) can undergo intracomplex CR (rate constant $^{app}k_b$) but also is free to dissociate $Fe^{2+}Cc$ with apparent dissociation rate constant $^{app}k_{off(2+)}$ and recombine with association rate constant $^{app}k_{on(2+)}$.

DOI: 10.1021/bi500888y
Biochemistry 2015, 54, 1188−1197

Scheme 1

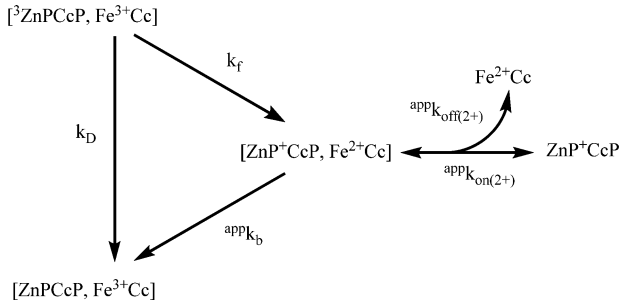

Each *individual* progress curve for **I** collected during an Fe^{3+}Cc titration can be well fit to Scheme 1 using numerical integration of the corresponding equations (Supporting Information), as shown in Figure 1. Moreover, as required, in the fit of each trace, the rate constant for the appearance of **I** (k_{rise} = 310 ± 12 s^{-1}) corresponds to the rate constant (k_2) for the decay of the triplet state in the bound complex. However, during a titration via the addition of up to 5 equiv of Cc per ZnPCcP, fit parameter $^{app}k_{off(2+)}$ increases linearly, by a factor of 6, while $^{app}k_b$ decreases by $^1/_3$, from ~60 to ~40 s^{-1} (Figure 3),

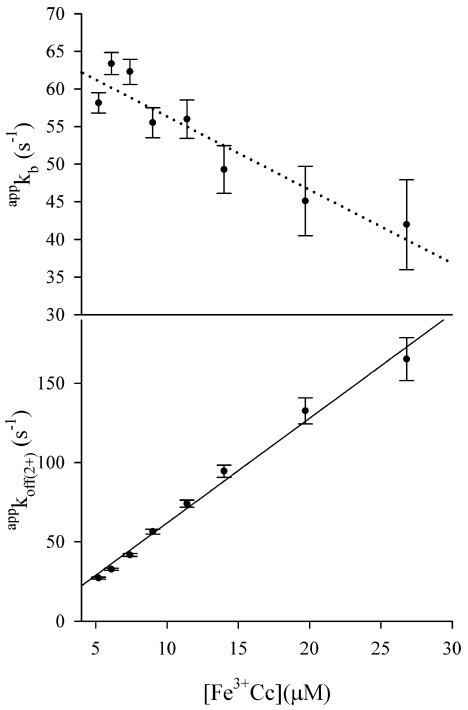

Figure 3. Titration of a sample of ~5 μM ZnPCcP with Fe^{3+}Cc (5–26 μM). (Top) $^{app}k_b$ through the titration. Dotted line to guide the eye. (Bottom) $^{app}k_{off(2+)}$ through the titration with a fit to eq 2 (black line). Conditions: 10 mM KP$_i$ buffer (pH 7), 20 °C.

with the main changes occurring well beyond the point at which ZnPCcP is fully bound. The fits to Scheme 1 further yield a systematic decrease in $^{app}k_{on(2+)}$ from ~1.4 × 10^7 to ~8 × 10^6 M^{-1} s^{-1}. However, a large uncertainty introduced by the limitation of data collection to 1 s, before all the intermediate has recombined, precludes detailed analysis. If Scheme 1 were adequate to describe the behavior of **I**, all three rate constants, $^{app}k_b$, $^{app}k_{off(2+)}$, and $^{app}k_{on(2+)}$, would remain invariant during the titration; only the amplitude of the signal would change, rising with the fraction of bound complex, and this would reach an unchanging maximum when all ZnPCcP was complexed. The progress curves for **I** show none of these characteristics.

The changes in CR rate constants beyond complete formation of the 1:1 complex instead reflect the presence of a ternary charge-separated complex and thus complement the finding that a description of triplet quenching requires the presence of a ternary photoexcited complex. To understand how to incorporate a ternary charge-separated complex into Scheme 1, it is important to consider all the processes that the binary charge-separated complex, **I**2(2+), can undergo following its formation through the dominant CS process. If this complex dissociates before CR can occur, the free ZnP$^+$CcP thus formed must rebind Fe^{2+}Cc to undergo CR, but instead, it can bind Fe^{3+}Cc, which acts as an "inhibitor" of charge recombination by taking the place of the Fe^{2+}Cc (the equilibrium binding constants for the association of Fe^{3+}Cc and Fe^{2+}Cc with WT CcP are similar[30]). Such an inhibited complex can further bind a second Fe^{3+}Cc to form a "doubly inhibited" ternary inhibitor [ZnP$^+$CcP, (Fe^{3+}Cc)$_2$] ≡ **I**3(3+/3+); it is the progressive accumulation of these species with an increasing [Fe^{3+}Cc] that acts to slow CR.

In addition to undergoing CR or dissociating, **I**2(2+) also can bind an Fe^{3+}Cc to form the **I**3(2+/3+) ternary complex. There are multiple possible alternative structures of such a ternary complex. Depending on the CR pathways within such a ternary complex and the probabilities of releasing Fe^{3+}Cc to re-form **I**2(2+) or of releasing Fe^{2+}Cc to form **I**2(3+), formation of **I**3(2+/3+) could either enhance or suppress CR as revealed by changes in $^{app}k_{off(2+)}$ and $^{app}k_b$ beyond 1 equiv of Fe^{3+}Cc. To address these issues, two types of "competition" titrations were performed.

Fe^{2+}Cc Titration. Assignment of the slower decay phase of **I** to accumulation of "inhibited" complex **I**2(3+), which cannot undergo CR, implies that addition of excess Fe^{2+}Cc should enhance the regeneration of ET-active **I**2(2+), thereby speeding CR and decreasing the lifetime of **I**. To examine this prediction, Fe^{2+}Cc was titrated into a 1:1 mixture of ~5 μM ZnPCcP and ~5 μM Fe^{3+}Cc [10 mM KP$_i$ buffer (pH 7), 20 °C] to a final concentration of added Fe^{2+}Cc of 22 μM. The fraction of photoexcited ^{3}ZnPCcP bound in complex with Fe^{3+}Cc (Figure S2 of the Supporting Information), as determined from biexponential fits of the triplet decay traces with rate constants k_1 and k_2 (Figure S3 of the Supporting Information), decreased throughout the titration, establishing that Fe^{3+}Cc and Fe^{2+}Cc bind to ZnPCcP/^{3}ZnPCcP with similar affinities.

The excess Fe^{2+}Cc also alters the time course for **I** (Figure 4). The trace for **I** generated without addition of Fe^{2+}Cc, which reproduces the corresponding trace of Figure 1, exhibits a slow phase of roughly 50% of the signal. As expected, progressive additions of Fe^{2+}Cc decrease the intensity of the signal for **I** but have little effect on its rate of appearance (k_{rise} = 370 ± 16 s^{-1}), which corresponds to the unvarying rate constant for triplet decay (k_2). However, added Fe^{2+}Cc obviously suppresses the slow component of CR, as anticipated.[d]

In fits of these curves to Scheme 1, "intracomplex" CR rate constant $^{app}k_b$, associated with the more rapidly decaying phase, decreases by ~$^1/_3$, from ~60 to <40 s^{-1} (Figure S4 of the Supporting Information), while the suppression of the slow component is manifest as an acceleration of decay, with the result being that the more slowly decaying component coalesces with the other (Figure 4). The observation that

DOI: 10.1021/bi500888y
Biochemistry 2015, 54, 1188–1197

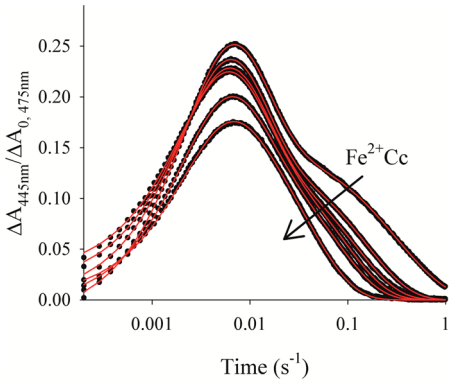

Figure 4. Titration of a sample of ~5 μM ZnPCcP and ~5 μM $Fe^{3+}Cc$ with 0−17 μM $Fe^{2+}Cc$. Progress curves for the charge-separated intermediate, **I**, normalized to A_0 of the corresponding decay at 475 nm (black) with fits to Scheme 1 (red). Conditions: 10 mM KP_i buffer (pH 7.0), 20 °C.

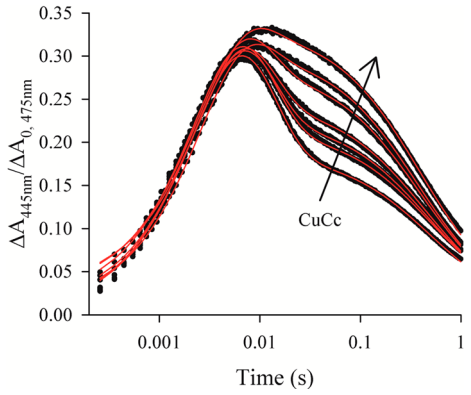

Figure 5. Titration of a sample of ~5 μM ZnPCcP and ~7 μM $Fe^{3+}Cc$ with 0−16 μM CuCc. Progress curves for the charge-separated intermediate, **I**, normalized to A_0 of the corresponding decay at 475 nm (black) with fits to Scheme 1 (red). Conditions: 10 mM KP_i buffer (pH 7.0), 20 °C.

increasing [$Fe^{2+}Cc$] accelerates CR confirms the basic tenet of Scheme 1, that **I**2(2+) dissociates, and that the slow CR phase is rate-limited by recombination of $Fe^{2+}Cc$ with ZnP^+CcP. Likewise, the apparent *decrease* in intracomplex CR rate constant $^{app}k_b$ with increasing [$Fe^{2+}Cc$] suggests that **I**2(2+) can bind a second $Fe^{2+}Cc$, forming a ternary **I**3(2+/2+) ≡ [ZnP^+CcP, $(Fe^{2+}Cc)_2$] complex. Apparently as a paradox, the binding of the second $Fe^{2+}Cc$ electron donor acts to decrease the net rate constant associated with $Fe^{2+}Cc \rightarrow ZnP^+CcP$ charge-recombination ET. This, however, simply implies that neither $Fe^{2+}Cc$ in **I**3(2+/2+) adopts the favorable bound conformation of the ET-active **I**2(2+) binary complex, while the observation that the fast phase decays exponentially indicates that **I**2(2+) and **I**3(2+/2+) are in rapid exchange. As discussed in more detail below, a parallel decrease in $^{app}k_{off(2+)}$ with [$Fe^{2+}Cc$] (Figure S5 of the Supporting Information), in contrast to an increase with [$Fe^{3+}Cc$] (see above) and [CuCc] (below), is further evidence of the inhibiting effect of the latter two Cc's. As with the $Fe^{3+}Cc$ titration, the $^{app}k_{on(2+)}$ values could not be further analyzed.

CuCc Titration. To test whether the increases in $^{app}k_{off(2+)}$ during the titration with $Fe^{3+}Cc$ and $Fe^{2+}Cc$ are caused exclusively by formation of the ternary complex through binding of an inert Cc, and not in some part through a self-exchange between bound $Fe^{3+}Cc$ and $Fe^{2+}Cc$, we performed an analogous titration with redox-inert CuCc.[19] CuCc was titrated into a sample of ~5 μM ZnPCcP and ~7 μM $Fe^{3+}Cc$ [10 mM KP_i buffer (pH 7), 20 °C] to a final concentration of ~16 μM CuCc. Inspection of the triplet decay traces (Figure S6 of the Supporting Information) shows a small increase in the lifetime of ^3ZnPCcP, an indication that the inert CuCc was replacing $Fe^{3+}Cc$ in the photoexcited complex, but the effect is too small to precisely quantify. The overall behavior of **I** during a titration with CuCc (Figure 5) is similar to that during the $Fe^{3+}Cc$ titration (Figure 1), with a k_{rise} of 300 ± 20 s^{-1}. However, fits of the **I** time courses with Scheme 1 reveal that as with the $Fe^{3+}Cc$, $^{app}k_{off(2+)}$ increases linearly with progressive additions of CuCc (Figure S7 of the Supporting Information), establishing the formation of ternary complex **I**3(2+/Cu) ≡ [ZnP^+CcP, $Fe^{2+}Cc$, CuCc]; again, $^{app}k_{on(2+)}$ values were not further analyzed. We observe a modest but significant decrease in $^{app}k_b$ with an increase in [CuCc] (Figure S8 of the Supporting Information), directly confirming that in the ternary complex the presence of the second, nonreactive Cc makes the $Fe^{2+}Cc$ less reactive. We return to this finding in the Discussion.

Core Kinetic Scheme. The experiments described above yield mechanistic constraints to guide expanding Scheme 1 to develop a core kinetic model of the ET photocycle for $Fe^{3+}Cc$ and ZnPCcP(W191F) as these proteins form dynamic binary and ternary complexes whose dissociation and combination occur on the long time scale of direct heme−heme ET in the CcP(W191F), FeCc complexes. These constraints and the modification that follow may be summarized.

(a) Dissociation/reassociation competes with ET during charge recombination; Scheme 1 includes dissociation of the binary CS intermediate, **I**2(2+).

(b) The ZnP^+CcP liberated upon dissociation of **I**2(2+) can bind $Fe^{3+}Cc$ to form the "inhibited" complex, **I**2(3+), slowing the second-order recombination process of the slow CR component. Scheme 1 must be extended to include formation of **I**2(3+) ≡ [ZnP^+CcP, $Fe^{3+}Cc$].

(c) An MCc (M = Fe^{2+}, Fe^{3+}, or Cu) can interact with **I**2(2+) to form a ternary complex whose structure is less suited to ET than that of the binary complex; to describe the "normal" titration of ZnPCcP by $Fe^{3+}Cc$, Scheme 1 must be modified to include the formation of the ternary complex, **I**3(2+/3+), which is allowed to dissociate either of the Cc to form one of two binary complexes, **I**2(2+) or **I**2(3+).

Scheme 2 presents a core kinetic model for the ZnPCcP-(W191F) and $Fe^{3+}Cc$ ET photocycle that incorporates these features and in fact represents a subset of Scheme S1 of the Supporting Information: k_{on} and $k_{off(2+/3+)}$ are the association and dissociation rate constants, respectively, for the binary complexes; $^{ter}k_{on(2+/3+)}$ and $^{ter}k_{off(2+/3+)}$ are rate constants for formation and dissociation of the ternary complex; all are provisionally taken to be identical for the photoexcited and charge-separated complexes but unique for each $Fe^{2+}Cc$ and $Fe^{3+}Cc$. Again, the CR rate constant for the binary complex is k_b; in principle, the ternary complex can also undergo CR, with rate constant $^{ter}k_b$. The scheme does not explicitly include the **I**3(3+/3+) complex because it cannot be kinetically differentiated from the "inhibitor" complex, **I**2(3+). Analogous schemes for the $Fe^{2+}Cc$ and CuCc titration ET photocycles are given by Schemes S2 and S3 of the Supporting Information.

In Scheme 2, **I**2(2+) can dissociate after photoinitiated CS ET, with rate constant $k_{off(2+)}$, and the liberated ZnP^+CcP is free

DOI: 10.1021/bi500888y
Biochemistry 2015, 54, 1188−1197

Scheme 2

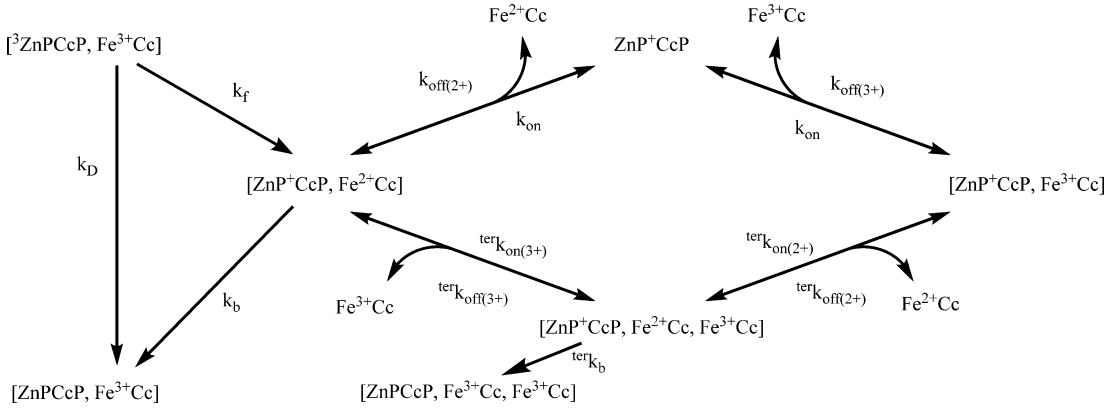

to bind nonreactive $Fe^{3+}Cc$ molecules, thereby forming the "inhibitor" complex, **I**2(3+),[e] and given that $[Fe^{3+}Cc] \gg [ZnP^{+}CcP]$, we infer that $ZnP^{+}CcP$ spends the majority of the time in a complex. Alternatively, **I**2(2+) can bind a second $Fe^{3+}Cc$ molecule to generate the ternary complex, **I**3(2+/3+), which can dissociate either Cc, re-forming **I**2(2+) or the inhibited binary complex, **I**2(3+). This process effectively enhances the apparent rate of dissociation of $Fe^{2+}Cc$ from **I**2(2+) by providing an additional route to form the inhibited complex, **I**2(3+), and it causes the concentration-dependent increase in the apparent rate constant, ${}^{app}k_{off(2+)}$, for CuCc and $Fe^{3+}Cc$ but a decrease for $Fe^{2+}Cc$, as noted above, amplifying the slow phase of CR.

Even an attempt to fit titration data with Scheme 2, a subscheme of the full kinetic scheme (Scheme S1 of the Supporting Information), presents formidable difficulties because of the large number of parameters and the impossibility of independently monitoring the individual $ZnP^{+}CcP$ species within Scheme 2: transient absorbance spectroscopy monitors only the sum of the charge-separated species. However, we can obtain parameters partially describing Scheme 2 by identifying them with the parameters obtained by fitting the progress curves to Scheme 1. The two critical parameters in Scheme 2 and Schemes S2 and S3 of the Supporting Information are $k_{off(2+)}$ and ${}^{ter}k_{on(M)}$ (M = Fe^{2+}, Fe^{3+}, or Cu), the rate constants for the processes that form the species $ZnP^{+}CcP$ and $[ZnP^{+}CcP, Fe^{2+}Cc, MCc] \equiv$ **I**3(2+/M), respectively, which represent the slower decay phase. Perhaps surprisingly, both a dissociation constant and an association constant can be obtained from the two parameters that describe the linear dependence of the *apparent* rate constant for the dissociation of **I**2(2+) of Scheme 1 (denoted ${}^{app}k_{off(2+)}$) on the concentration of added titrant, $[MCc]_0$, as found in the fits to Scheme 1. The correlation can be written as follows.

$$ {}^{app}k_{off(2+)} = k_{off(2+)} + {}^{ter}k_{on(M)}[MCc]_0 \quad (1) $$

First, the concentration of titrant MCc is much greater than the concentration of **I**2(2+) at all times during a photocycle ($[MCc] \gg$ **I**2(2+)), so one may equate the instantaneous value of free [MCc] with the total concentration ($[MCc] \approx [MCc]_0$). As a result, in Scheme 2, the formation of the ternary complex, **I**2(2+) + MCc → **I**3(2+/M), is pseudo-first-order. Second, this *formation* of **I**3(2+/M) manifests itself through the description of the titrations with Scheme 1 as a contribution to the apparent rate constant for **I**2(2+) *dissociation* that increases with $[MCc]_0$ during a titration ($\Delta^{app}k_{off(2+)} = {}^{ter}k_{on(M)}[MCc]_0$). Addition of this contribution to the true rate constant for dissociation, $k_{off(2+)}$, leads to eq 1.[f]

The variations of ${}^{app}k_{off(2+)}$ with $[MCc]_0$ obtained through analysis of the $Fe^{3+}Cc$ and CuCc titrations with Scheme 1 and their description with eq 1 yield the values of ${}^{ter}k_{on(M)}$ listed in Table 2. These dissociation rate constants for the ternary complexes are approximately the same, confirming that the formation of a ternary complex is the cause of the concentration dependence of the apparent dissociation of the binary complex, ${}^{app}k_{off(2+)}$.

Table 2. Kinetic Parameters for Linear Fits of ${}^{app}k_{off(2+)}$[a]

protein titrant	${}^{ter}k_{on(M)}$ (M^{-1} s^{-1})
$Fe^{3+}Cc$	$(6.6 \pm 0.7) \times 10^6$
CuCc	$(6.9 \pm 0.2) \times 10^6$

[a]Values shown with 95% confidence intervals.

DISCUSSION

Introduction of the W191F mutation greatly slows the CR "half" of the ET photocycle associated with the [ZnPCcP, $Fe^{3+}Cc$] complex by eliminating fast hole hopping from $Fe^{2+}Cc$ to the ZnP cation radical in $ZnP^{+}CcP$ through W191.[9] This mutation both enhances the accumulation of the CS intermediate, **I**, and greatly extends the time scales over which binding and dissociation of this paradigmatic protein−protein ET pair can be probed through ET photocycle measurements. This study reports progress curves for the triplet decay and charge-separated intermediate curves of the titration of ZnPCcP(W191F) with $Fe^{3+}Cc$, as well as titrations of the [ZnPCcP, $Fe^{3+}Cc$] complex at fixed concentration with $Fe^{2+}Cc$ and with CuCc. The results of these experiments require an expansion of the CR branch of the simple photocycle for intracomplex ET between ZnPCcP(W191F) and $Fe^{3+}Cc$ (Scheme 1) to incorporate (i) dissociation/recombination of the charge-separated intermediate state; (ii) two types of binary intermediate complexes, the reactive intermediate, **I**2(2+), and the "inhibited" complex, **I**2(3+); and (iii) the ternary intermediate complex in which $ZnP^{+}CcP$ binds both $Fe^{2+}Cc$ and $Fe^{3+}Cc$, **I**3(2+/3+) (Scheme 2). Incorporation of this expanded CR scheme within the ET photocycle formalizes and expands earlier proposals to explain apparently anomalous kinetic and binding measurements[20,31] and further allows us to introduce a distinctive perspective on the structure of the ternary CS complex.

DOI: 10.1021/bi500888y
Biochemistry 2015, 54, 1188−1197

An early proposal suggested that "substrate-assisted product dissociation" added a concentration-dependent term to the dissociation of Cc from CcP.[20] Such a term offered an explanation for observed steady state turnover rates at high protein concentrations that were greater than the dissociation rate constants reported at low concentrations. Those results yielded a [Cc]-dependent, second-order dissociation rate constant in agreement with an earlier proton NMR study[31] that observed concentration-dependent exchange rates between free Cc and Cc bound to CcP: an increase in the absolute protein concentration at a constant CcP:Cc ratio shifted the exchange from slow exchange on the NMR time scale to fast exchange.[31] The measurements of the CS recombination kinetics presented here show a corresponding concentration-dependent increase in the apparent rate of dissociation of the binary CS complex, **I**2(2+).

Stopped-flow measurements[21,32] also were interpreted in terms of a concentration dependence of the apparent dissociation of the binary complex, caused by transient formation of the ternary complex in which binding at the reactive site is decreased by repulsion between bound Cc. The detailed kinetic Scheme 2 correspondingly incorporates the reaction between **I**2(2+) and an additional $Fe^{3+}Cc$ to form the weakly bound ternary complex, **I**3(2+/3+), which is free to release *either* $Fe^{2+}Cc$ or $Fe^{3+}Cc$. When the kinetics of charge recombination are interpreted within the contracted kinetic Scheme 1, which does not explicitly include **I**3(2+/3+), the influence of the additional channel for liberating $Fe^{2+}Cc$ by dissociation from the ternary complex is manifest as an enhancement of the *apparent* dissociation constant of **I**2(2+) and leads to the appearance of "substrate-assisted product dissociation".[20] However, to understand these results and most especially the strength and effects of Cc repulsion within the ternary complex, it is necessary to incorporate the contributions of repulsion into the thermodynamics of binding within a two-site binding model.

Thermodynamics of Two-Site Binding. It is well-known that binding measurements for a system that includes binary and ternary complexes provide only two thermodynamic affinity constants.[33] These can be formulated as one constant for the binding to CcP of one Cc to form a binary complex, K_I, and the second constant for the binding of a second Cc to form the ternary complex, K_{II}, with free energies ΔG_I and ΔG_{II}, respectively.

$$CcP + Cc \overset{K_I}{\rightleftharpoons} [CcP, Cc] \tag{2}$$

$$[CcP, Cc] + Cc \overset{K_{II}}{\rightleftharpoons} [CcP, Cc_2] \tag{3}$$

Alternatively, the second constant can be defined as that for the direct binding of two Cc's by CcP, affinity constant $K_T = K_I K_{II}$, a formulation that is seen below to be particularly useful for our discussion.

$$CcP + 2Cc \overset{K_T}{\rightleftharpoons} [CcP, Cc_2] \tag{4}$$

It is also well-known that the two constants K_I and K_{II} of eqs 2 and 3, respectively, are *not* site binding constants,[33] nor do they imply *any* specific binding model. Nonetheless, it is also well-known that the thermodynamic formulation *formally* corresponds to *independent* binding at two preexisting sites, 1 and 2, with binding constants K_1 and K_2, respectively, where $K_I = K_1 + K_2$ and $K_{II} = K_1K_2/(K_1 + K_2)$[34] regardless of *whether* the system is physically represented by this model. In fact, calculations and experiments have confirmed that the two Cc's cannot bind independently and that the stability of the ternary complex is diminished by electrostatic repulsions between the two positively charged Cc's (anticooperative binding).[35,36]

To describe the thermodynamics of two-site binding of two Cc's by CcP, we consider two CcP binding sites, 1 and 2, where Cc can bind to form alternative binary complexes with true site constants K_1 and K_2, respectively, and binding free energies ΔG_1 and ΔG_2, respectively

$$-RT \ln K_i = \Delta G_i \quad i = 1, 2 \tag{5}$$

as illustrated in Figure 6A. With regard to the formation of the ternary complex, (i) electrostatic repulsion between the two

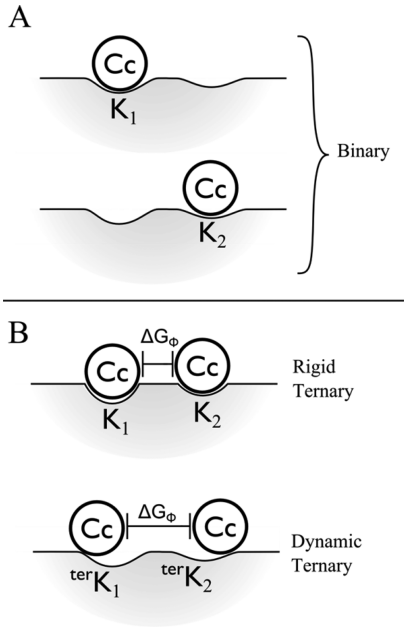

Figure 6. Representations of Cc bound to the surface of CcP within the binary and ternary complexes. (A) Two unique binary complexes with equilibrium affinity constants K_1 and K_2. (B) Rigid and dynamic models of the ternary complex with incorporated free energy of repulsion ΔG_Φ.

bound Cc molecules of the ternary complex necessarily causes the binding to be "anticooperative" and can be captured by explicitly introducing a free energy of repulsion ($\Delta G_\Phi > 0$) into the free energy for formation of the ternary complex from its unbound components (eq 6, ΔG_T).

$$-RT \ln K_T = \Delta G_T = {}^{ter}\Delta G_1 + {}^{ter}\Delta G_2 + \Delta G_\Phi \tag{6}$$

(ii) The free energies of binding of a Cc to the CcP surface at each site *within the ternary complex* need not have the same values as those for the two binary complexes, *namely*, in general $\Delta G_i \neq {}^{ter}\Delta G_i$. This is so because upon binding of a second Cc to CcP, the binding geometries at both sites and even the protein charges can adjust to create the most stable ternary complex: when the total free energy of the ternary complex, ΔG_T, is minimized, a diminution in the free energies of binding to the CcP surface can be more than compensated by mitigation of the repulsion, as shown in Figure 6B. In different terms, the ternary complex can lose free energy of interfacial binding interactions but benefit overall by a more than compensating decrease in repulsion.

DOI: 10.1021/bi500888y
Biochemistry 2015, 54, 1188−1197

To understand the role of repulsions in the ternary complex between CcP and Cc quantitatively, it is nonetheless useful to first consider anticooperative binding in the *rigid limit* of the two-site model, where the site binding constants, K_1 and K_2, are *assigned* as being unchanged upon binding of a second Cc, and thus, the site-binding free energies within the ternary complex ($^{ter}\Delta G_i$, i = 1, 2) are assigned to equal those within the binary complexes ($\Delta G_i = {}^{ter}\Delta G_{,i}$) (Figure 6B). Anticooperativity is introduced by repulsion between the two Cc's, decreasing K_{II}, through the incorporation of a repulsion factor $\Phi = e^{-\Delta G_\Phi/RT}$. In this limit, the relationship between the measured affinity constants, K_I and K_T, and the site-affinity constants, K_1 and K_2, and the free energy for forming the ternary complex from its components then become

$$K_I = K_1 + K_2 \tag{7}$$

$$K_T = K_1 K_2 \Phi \tag{8}$$

$$-RT \ln K_T = \Delta G_T = \Delta G_1 + \Delta G_2 + \Delta G_\Phi \tag{9}$$

Kinetic measurements and mutagenesis, both in our laboratory[8,37−39] and the laboratories of others,[12,40−42] generally arrived at measured affinity constants for the "first" and "second" Cc, which correspond to thermodynamic constants of $K_I \sim 10^7$ M^{-1} and $K_{II} \sim 10^4$ M^{-1}, respectively, at 10 mM potassium phosphate buffer (pH 7) and 20 °C, values corroborated by the study presented here. Use of these consensus values permits us to discuss the actual site constants and to set limits on the repulsion free energy.

The fact that the crystal and NMR[43−45] structures reveal a 1:1 CcP/Cc complex with similar conformations would *seem* to suggest that one binding site (site 1) is overwhelmingly more favorable that any second site. However, in the extreme case of this rigid limit, if the site constants were equal to the measured thermodynamic affinity constants ($K_1 \approx K_I$, and $K_2 \approx K_{II}$), then repulsion would be zero, and this is ruled out by the measurements of Erman and co-workers,[36] as noted above. This requires that the actual site-binding constant K_2 must be larger than the measured value of K_{II} (10^4), although still sufficiently smaller than K_1 that the binary complex is predominantly in the tightly binding form in accordance with the NMR studies.[44] We propose that if K_2 were merely 10-fold less than K_1, rather than the 10^3-fold that would apply if one inappropriately assigned $K_2 = K_{II}$, then it is likely that the binary complex with binding at site 1, the "tight" site, would dominate both the crystallization process that led to the X-ray structure and the solution structures. If we then use this assumption within eqs 7 and 8 for concreteness, yielding the plausible value $K_2 \sim 10^6$, then one arrives at a calculated repulsion constant Φ of $\approx 10^{-2}$, corresponding to ΔG_Φ = 2.7 kcal/mol. If one further relaxes the *rigid limit* two-site model, allowing the Cc at each site within the ternary complex to adjust its binding conformation relative to that of the binary complex, this further weakens the possible influence of repulsions. Such relaxation leads to the inequalities $^{ter}K_1 < K_1$ and $^{ter}K_2 < K_2$; through eq 7, this in turn would correspondingly reduce the free energy of repulsion (ΔG_Φ < 2.7 kcal/mol).

We may conclude this discussion by noting that eq 7 places an upper limit on the affinity at the weaker binding site ($K_2 = K_1 = K_I/2 = 5 \times 10^6$). This limiting value in turn leads to an absolute upper bound to the repulsion free energy in *any* two-site model, through the use of eq 8. Use of the consensus measured thermodynamic affinity constants and this upper bound of K_2 within the *rigid limit* two-site model gives an upper bound to the repulsion free energy at 10 mM KP_i buffer (pH 7) at 20 °C: $\Delta G_\Phi \leq 3.3$ kcal/mol; this is an absolute upper bound, as relaxation of the rigid limit would only lower this value. The experiments designed to probe the repulsion free energy, which employed a ternary complex that constrains the movement of one Cc, yielded a free energy for the repulsion between the two Cc's (ΔG_Φ) of 6 kcal/M, roughly twice the actual upper limit for the noncovalent ternary complex revealed by the present thermodynamic analysis.[36] However, those experiments were conducted at lower ionic strengths and higher pHs and temperatures [10 mM *ionic strength* KP_i buffer (pH 7.5) at 25 °C]; all of these differences would enhance repulsion. Thus, we suggest that the two measurements are satisfactorily supportive.

Nature of Binary and Ternary Complexes. Despite the beautiful visualization of complementary docking between CcP and Cc provided by the crystal structure, there is good reason to believe that this structure is actually a member of an ensemble of solution binding configurations, as suggested long ago by Brownian dynamics simulations.[40] Such a situation was supported by the "Velcro" model in which a large surface region, or charged patch, on CcP participates in complex formation[46] and, most persuasively, has recently been underscored by the NMR studies of Ubbink and co-workers, who found that within the binary complex, Cc spends up to 30% of its time in an encounter complex with CcP as a collection of nonspecific binding configurations around the "tight" site.[22] Consistent with this view, small and subtle changes in the binding surfaces of Cc and CcP introduced by point mutations significantly change the structure of the docked complex.[6] Collectively, these measurements lead to an expanded, more dynamic view of the association between CcP and a single Cc in solution. This thermodynamic analysis of binding extends such ideas by showing that the second binding site has a much greater affinity than previously recognized. Stronger second-site binding would in turn contribute to a broader ensemble of binary structures.

Combining the analysis of affinities with the kinetic measurements of the charge-recombination process further contributes to our understanding of the structure of the ternary complex, and to the view that it is even more dynamic than the binary complex, and that the most probable binding sites and/or geometries for the two Cc's not necessarily identical to those most characteristic of the alternative binary complexes. This picture is supported by our experimental observation that increasing concentrations of MCc not only increase $^{app}k_{off(2+)}$ but also decrease $^{app}k_b$. If the two Cc's within the ternary complex, **I**3(2+/3+) and **I**3(2+/Cu), were situated as in the corresponding binary complexes, the $^{app}k_b$ would remain constant, contrary to observation; only $^{app}k_{off(2+)}$ (and possibly $^{app}k_{on}$) would change. Instead, the presence of both binary and ternary complexes [**I**2(2+) and **I**3(2+/3+), respectively] in rapid exchange generates an observed $^{app}k_b$ that is a weighted average of k_b and $^{ter}k_b$. The finding that $^{app}k_b$ decreases with an increasing concentration of the ternary complex indicates that the presence of the second Cc forces the Fe^{2+}Cc to bind in a less reactive conformation than in the binary complex, and the inequality $0 < {}^{ter}k_b < k_b$.[g]

In conclusion, we have developed a generalized kinetic scheme for the ET photocycle of the complex between ZnPCcP-(W191F) and Fe^{3+}Cc that formalizes, expands, and revises the picture of the kinetic behavior and structure of the charge-separated intermediate. The resulting kinetic Scheme 2

DOI: 10.1021/bi500888y
Biochemistry 2015, 54, 1188−1197

incorporates binary complexes in two different redox states, I2(2+) and I2(3+), along with a ternary complex, I3(2+/3+), and accounts for the dynamics of complex interconversion over time scales from microseconds to seconds. In formalizing and enhancing earlier proposals of "substrate-assisted product dissociation", we have developed a thermodynamic description of two-site binding that reveals that Cc binds at the weaker binding site with much greater affinity than previously recognized and places upper bounds on the contributions of repulsion between the two Cc's of the ternary complex. In conjunction with recent NMR studies, the analysis further suggests a dynamic view of the ternary complex, wherein neither Cc necessarily faithfully adopts the crystal structure configuration because of Cc−Cc repulsion.

■ ASSOCIATED CONTENT

Supporting Information

Triplet decay curves with fits for the Fe^{3+}Cc titration, fit parameters for Fe^{2+}Cc and CuCc intermediate progress curves to Scheme 1, extended and modified kinetic schemes used to analyze Fe^{2+}Cc and CuCc titration intermediate curves, comparisons of triplet decay rate constants for the Fe^{2+}Cc titration, and details of equations for the global triple-exponential equation and the system of differential equations used in Scheme 1. This material is available free of charge via the Internet at http://pubs.acs.org.

■ AUTHOR INFORMATION

Corresponding Author

*E-mail: bmh@northwestern.edu. Phone: (847) 491-3104.

Funding

We gratefully acknowledge the support of the National Institutes of Health (HL 63203).

Notes

The authors declare no competing financial interest.

■ ACKNOWLEDGMENTS

We thank Dr. Judith Nocek and Dr. Diana Mayweather for many useful discussions and Dr. John Magyar for providing protocols used in the preparation of CuCc. We further acknowledge two anonymous reviewers, whose incisive comments and suggestions directly led to major improvements in this work.

■ ABBREVIATIONS

ET, electron transfer; CcP, cytochrome *c* peroxidase; Cc, cytochrome *c*; ZnPCcP, Zn-protoporphyrin IX-substituted CcP; CS, charge separation; CR, charge recombination.

■ ADDITIONAL NOTES

[a]For the sake of brevity when discussing the various forms of **I**, we include additional descriptors. Thus, **I2** refers to a binary complex and **I3** to a ternary complex, and the state of the Cc(s) bound is further specified within parentheses. Thus, **I2**(2+) refers to the binary complex [ZnP^+CcP, Fe^{2+}Cc], while **I3**(2+/Cu) refers to the ternary complex [ZnP^+CcP, Fe^{2+}Cc, CuCc].

[b]The decay with rate constant k_2 represents both electron (k_f) and energy transfer. We roughly estimate that the quenching is up to 85% energy transfer based on empirical absorbance measurements.

[c]From empirical analysis of previously published data (not shown), we roughly estimate the maximal concentration of ZnP^+CcP to be ∼0.2 μM when $[Fe^{3+}Cc]_0 = [ZnPCcP]_0 = 5$ μM.

[d]With progressive additions of $[Fe^{2+}Cc]$, the slowly decaying phase of the intermediate progress curve becomes pseudo-first-order, as expected when $[Fe^{2+}Cc] \gg [ZnP^+CcP]$, and it can be fit with an analytical function with an exponential rise and fall. However, to maintain comparisons with the analysis of the other titrations, we have chosen to continue to use Scheme 1.

[e]An increasing level of accumulation of **I2**(3+) with added Fe^{3+}Cc, which is unavailable for CR, is expected to cause a decrease in $^{app}k_{on(2+)}$ as observed.

[f]Because the concentration of ternary complex **I3**(2+/3+) is roughly 1 order of magnitude lower than that of the binary complex, and it is shown above that CR in the ternary complex is slower than in the binary complex ($^{ter}k_b < k_b$), we may ignore CR within the ternary complex to obtain a semiquantitative analysis of $^{app}k_{off(2+)}$.

[g]A more restrictive limit on $^{ter}k_b$ could not be established, given the available range of Fe^{3+}Cc concentrations.

■ REFERENCES

(1) Bendall, D. S. (1996) *Protein electron transfer*, BIOS Scientific Publishers, Oxford, U.K.

(2) Satterlee, J. D., Moench, S. J., and Erman, J. E. (1987) A proton NMR study of the non-covalent complex of horse cytochrome *c* and yeast cytochrome-*c* peroxidase and its comparison with other interacting protein complexes. *Biochim. Biophys. Acta 912*, 87−97.

(3) Yi, Q., Erman, J. E., and Satterlee, J. D. (1994) {+1}H NMR evaluation of yeast isozyme-1 ferricytochrome *c* equilibrium exchange dynamics in noncovalent complexes with two forms of yeast cytochrome *c* peroxidase. *J. Am. Chem. Soc. 116*, 1981−1987.

(4) Volkov, A. N., Nicholls, P., and Worrall, J. A. (2011) The complex of cytochrome c and cytochrome c peroxidase: The end of the road? *Biochim. Biophys. Acta 1807*, 1482−1503.

(5) Pelletier, H., and Kraut, J. (1992) Crystal structure of a complex between electron transfer partners, cytochrome *c* peroxidase and cytochrome *c*. *Science 258*, 1748−1755.

(6) Kang, S. A., and Crane, B. R. (2005) Effects of interface mutations on association modes and electron-transfer rates between proteins. *Proc. Natl. Acad. Sci. U.S.A. 102*, 15465−15470.

(7) Goodin, D. B., Mauk, A. G., and Smith, M. (1987) The peroxide complex of yeast cytochrome *c* peroxidase contains two distinct radical species, neither of which resides at methionine 172 or tryptophan 51. *J. Biol. Chem. 262*, 7719−7724.

(8) Nocek, J. M., Zhou, J. S., De Forest, S., Priyadarshy, S., Beratan, D. N., Onuchic, J. N., and Hoffman, B. M. (1996) Theory and practice of electron transfer within protein-protein complexes: Application to the multi-domain binding of cytochrome *c* by cytochrome *c* peroxidase. *Chem. Rev. 96*, 2459−2489.

(9) Seifert, J. L., Pfister, T. D., Nocek, J. M., Lu, Y., and Hoffman, B. M. (2005) Hopping in the electron-transfer photocycle of the 1:1 complex of Zn-cytochrome c peroxidase with cytochrome c. *J. Am. Chem. Soc. 127*, 5750−5751.

(10) Hildebrandt, P., English, A. M., and Smulevich, G. (1992) Cytochrome *c* and cytochrome *c* peroxidase complex as studied by resonance raman spectroscopy. *Biochemistry 31*, 2384−2392.

(11) Fox, T., Hazzard, J. T., Edwards, S. L., English, A. M., Poulos, T. L., and Tollin, G. (1990) Rate of intramolecular reduction of ferryl iron in compound I of cytochrome *c* peroxidase. *J. Am. Chem. Soc. 112*, 7426−7428.

(12) Kornblatt, J. A., and English, A. M. (1986) The binding of porphyrin cytochrome *c* to yeast cytochrome *c* peroxidase. A fluorescence study of the number of sites and their sensitivity to salt. *Eur. J. Biochem. 155*, 505−511.

(13) Hoffman, B. M., Natan, M. J., Nocek, J. M., and Wallin, S. A. (1991) Long-range electron transfer within metal-substituted protein complexes. *Struct. Bonding (Berlin, Ger.) 75*, 85−108.

DOI: 10.1021/bi500888y
Biochemistry 2015, 54, 1188−1197

(14) Ho, P. S., Hoffman, B. M., Kang, C. H., and Margoliash, E. (1983) Control of the transfer of oxidizing equivalents between heme iron and free radical site in yeast cytochrome *c* peroxidase. *J. Biol. Chem. 258*, 4356−4363.
(15) Erman, J. E., and Vitello, L. B. (1998) Cytochrome c peroxidase: A model heme protein. *J. Biochem. Mol. Biol. 31*, 307−327.
(16) Mei, H., Wang, K., Peffer, N., Weatherly, G., Cohen, D. S., Miller, M., Pielak, G., Durham, B., and Millett, F. (1999) Role of configurational gating in intracomplex electron transfer from cytochrome c to the radical cation in cytochrome c peroxidase. *Biochemistry 38*, 6846−6854.
(17) Wallin, S. A., Stemp, E. D. A., Everest, A. M., Nocek, J. M., Netzel, T. L., and Hoffman, B. M. (1991) Multiphasic intracomplex electron transfer from cytochrome *c* to Zn cytochrome *c* peroxidase: Conformational control of reactivity. *J. Am. Chem. Soc. 113*, 1842−1844.
(18) Wang, J., Mauro, J. M., Edwards, S. L., Oatley, S. J., Fishel, L. A., Ashford, V. A., Xuong, N.-h., and Kraut, J. (1990) X-ray structures of recombinant yeast cytochrome *c* peroxidase and three heme-cleft mutants prepared by site-directed mutagenesis. *Biochemistry 29*, 7160−7173.
(19) Zhou, J. S., Nocek, J. M., DeVan, M. L., and Hoffman, B. M. (1995) Inhibitor-enhanced electron transfer: Copper cytochrome *c* as a redox-inert probe of ternary complexes. *Science 269*, 204−207.
(20) Zhang, Q., Wallin, S. A., Miller, R. M., Billstone, V., Spears, K. G., Hoffman, B. M., and McLendon, G. (1993) Thermodynamic and kinetic aspects of binding and recognition in the cytochrome *c* cytochrome *c* peroxidase complex. *J. Am. Chem. Soc. 115*, 3665−3669.
(21) Mei, H., Wang, K., McKee, S., Wang, X., Waldner, J. L., Pielak, G. J., Durham, B., and Millett, F. (1996) Control of formation and dissociation of the high-affinity complex between cytochrome c and cytochrome c peroxidase by ionic strength and the low-affinity binding site. *Biochemistry 35*, 15800−15806.
(22) Bashir, Q., Volkov, A. N., Ullmann, G. M., and Ubbink, M. (2010) Visualization of the encounter ensemble of the transient electron transfer complex of cytochrome c and cytochrome c peroxidase. *J. Am. Chem. Soc. 132*, 241−247.
(23) Volkov, A. N., Ubbink, M., and van Nuland, N. A. J. (2010) Mapping the encounter state of a transient protein complex by pre NMR spectroscopy. *J. Biomol. NMR 48*, 225−236.
(24) Teske, J. G., Savenkova, M. I., Mauro, J. M., Erman, J. E., and Satterlee, J. D. (2000) Yeast cytochrome c peroxidase expression in *Escherichia coli* and rapid isolation of various highly pure holoenzymes. *Protein Expression Purif. 19*, 139−147.
(25) Pollack, W. B. R., Rosell, F. I., Twitchett, M. B., Dumont, M. E., and Mauk, A. G. (1998) Bacterial expression of a mitochondrial cytochrome *c*. Trimethylation of lys72 in yeast iso-1-cytochrome *c* and the alkaline conformational transition. *Biochemistry 37*, 6124−6131.
(26) Yonetani, T. (1967) Studies on cytochrome *c* peroxidase. X. Crystalline apo- and reconsituted holoenzymes. *J. Biol. Chem. 242*, 5008−5013.
(27) Findlay, M. C., Dickinson, L. C., and Chien, J. C. W. (1977) Copper-cytochrome c. *J. Am. Chem. Soc. 99*, 5168−5173.
(28) Ho, P. S., Sutoris, C., Liang, N., Margoliash, E., and Hoffman, B. M. (1985) Species specificity of long-range electron transfer within the complex between zinc-substituted cytochrome *c* peroxidase and cytochrome *c*. *J. Am. Chem. Soc. 107*, 1070−1071.
(29) Northrup, S. H., Reynolds, J. C. L., Miller, C. M., Forrest, K. J., and Boles, J. O. (1986) Diffusion-controlled association rate of cytochrome *c* and cytochrome *c* peroxidase in a simple electrostatic model. *J. Am. Chem. Soc. 108*, 8162−8170.
(30) Mauk, M. R., Ferrer, J. C., and Mauk, A. G. (1994) Proton linkage in formation of the cytochrome c-cytochrome c peroxidase complex: Electrostatic properties of the high- and low-affinity cytochrome binding sites on the peroxidase. *Biochemistry 33*, 12609−12614.
(31) Moench, S. J., Chroni, S., Lou, B., Erman, J. E., and Satterlee, J. D. (1992) Proton NMR comparison of noncovalent and covalently cross-linked complexes of cytochrome *c* peroxidase with horse, tuna, and yeast ferricytochromes *c*. *Biochemistry 31*, 3661−3670.
(32) Miller, M. A., Geren, L., Han, G. W., Saunders, A., Beasley, J., Pielak, G. J., Durham, B., Millett, F., and Kraut, J. (1996) Identifying the physiological electron transfer site of cytochrome *c* peroxidase by structure-based engineering. *Biochemistry 35*, 667−673.
(33) Nocek, J. M., Leesch, V. W., Zhou, J. S., Jiang, M., and Hoffman, B. M. (2000) Multi-domain binding of cytochrome *c* peroxidase by cytochrome *c*: Thermodynamic vs. microscopic binding constants. *Isr. J. Chem. 40*, 35−46.
(34) Wyman, J. (1968) Regulation in macromolecules as illustrated by haemoglobin. *Q. Rev. Biophys. 1*, 35−80.
(35) Northrup, S. H., and Thomasson, K. A. (1992) Electrostatic calculations of 2:1 complexes of cytochrome *c* and cytochrome *c* peroxidase. *FASEB J. 6*, A474.
(36) Nakani, S., Vitello, L. B., and Erman, J. E. (2006) Characterization of four covalently-linked yeast cytochrome c/cytochrome c peroxidase complexes: Evidence for electrostatic interaction between bound cytochrome c molecules. *Biochemistry 45*, 14371−14378.
(37) Stemp, E. D. A., and Hoffman, B. M. (1993) Cytochrome *c* peroxidase binds two molecules of cytochrome *c*: Evidence for a low-affinity, electron-transfer-active site on cytochrome *c* peroxidase. *Biochemistry 32*, 10848−10865.
(38) Zhou, J. S., and Hoffman, B. M. (1994) Stern-volmer in reverse: 2:1 stoichiometry of the cytochrome *c* cytochrome *c* peroxidase electron-transfer complex. *Science 265*, 1693−1696.
(39) Leesch, V. W., Bujons, J., Mauk, A. G., and Hoffman, B. M. (2000) Cytochrome *c* peroxidase:cytochrome *c* complex: Locating the second binding domain on cytochrome *c* peroxidase with site-directed mutagenesis. *Biochemistry 39*, 10132−10139.
(40) Northrup, S. H., Boles, J. O., and Reynolds, J. C. L. (1988) Brownian dynamics of cytochrome *c* and cytochrome *c* peroxidase association. *Science 241*, 67−70.
(41) Kang, C. H., Ferguson-Miller, S., and Margoliash, E. (1977) Steady state kinetics and binding of eukaryotic cytochromes *c* with yeast cytochrome *c* peroxidase. *J. Biol. Chem. 252*, 919−926.
(42) Mei, H., Geren, L., Miller, M. A., Durham, B., and Millett, F. (2002) Role of the low-affinity binding site in electron transfer from cytochrome c to cytochrome c peroxidase. *Biochemistry 41*, 3968−3976.
(43) Guo, M., Bhaskar, B., Li, H., Barrows, T. P., and Poulos, T. L. (2004) Crystal structure and characterization of a cytochrome c peroxidase-cytochrome c site-specific cross-link. *Proc. Natl. Acad. Sci. U.S.A. 101*, 5940−5945.
(44) Volkov, A. N., Worrall Jonathan, A. R., Holtzmann, E., and Ubbink, M. (2006) From the cover: Solution structure and dynamics of the complex between cytochrome c and cytochrome c peroxidase determined by paramagnetic nmr. *Proc. Natl. Acad. Sci. U.S.A. 103*, 18945−18950.
(45) Bashir, Q., Volkov, A. N., Ullmann, G. M., and Ubbink, M. (2010) Visualization of the encounter ensemble of the transient electron transfer complex of cytochrome c and cytochrome c peroxidase. *J. Am. Chem. Soc. 132*, 241−247.
(46) McLendon, G. (1991) Control of biological electron transport via molecular recognition and binding: The "velcro" model. *Struct. Bonding (Berlin, Ger.) 75*, 159−174.

DOI: 10.1021/bi500888y
Biochemistry 2015, 54, 1188−1197